Evaluation of the Effect of Heat Input on Welded Joint Properties of ASTM A572 Grade 50 Steel Using the GMAW Process with 90Ar-10CO₂ Shielding Gas and Spray Metal Transfer

Álvaro Manuel Díaz Ávila[1] , Edinson de Jesús Herrera De Oro[1] , Elkin Camilo Medellín Pérez[1] , Enrique Esteban Niebles Núñez[2] ,
Jimy Unfried-Silgado[1]

[1] Universidad de Córdoba, Departamento de Ingeniería Mecánica, Grupo de Investigación Ingeniería, Ciencia y Tecnología – ICT, Montería, Colombia.

[2] Universidad Autónoma del Caribe, Grupo de Investigación en Materiales, Procesos y Tecnologías de Fabricación – IMTEF, Barranquilla, Colombia.

Abstract: In this study, the influence of heat input on the mechanical properties and microstructure of welded joints in ASTM A572 grade 50 steel using the GMAW process and 90Ar-10CO₂ shielding gas was investigated. Process parameters were varied between 20-30 V and 230-250 A, which were adjusted aiming to obtain spray transfer together producing two heat inputs with a 10% difference between them. Visual inspection, tensile tests, microhardness scans, measurements of the width of the heat-affected zone (HAZ), and metallography were performed. The experimental measurements were complemented by calculating the continuous cooling transformation (CCT) diagram of the steel from its chemical composition. The results showed that discontinuity-free and visually acceptable welded joints were obtained. The microstructure of the fusion zone was primarily composed of acicular ferrite, and the HAZ contained a mixture of bainite, pearlite, and ferrite as calculated by the CCT diagram. No statistically significant variations were observed in the microhardness measurements, with the highest value (240 MHV) obtained in the fusion zone. The width of the HAZ varied proportionally with the heat input, while no significant differences were found in the stress results as a function of the heat input.

Key-words: Carbon and low alloy steels; Mechanical properties of welded joints; Gas metal arc welding, Welding metallurgy.

1. Introduction

Since 2000, global steel production has significantly increased, reaching a record high of 1.7 billion metric tons in 2017. However, steel production accounts for 9% of global CO₂ emissions. According to the International Energy Agency (IEA), steel demand is projected to double by 2050. To reduce carbon emissions per unit of steel production or adopt alternative construction approaches [1], materials with a better strength-to-weight ratio have been introduced, with High-strength low-alloy (HSLA) steels standing out [2]. HSLA steels include minimal amounts of alloying elements (0.05-0.15% by weight), such as Mo, Nb, Ti, and V [3-5], and adding Nb to low-carbon steel can increase its strength by up to 50% [6,7]

HSLA steels have a tensile strength greater than 450 MPa and their ductility can reach up to 30%. The improvement in the mechanical properties of HSLA steels is mainly due to the added microalloys, which provide grain refinement strengthening, dislocations, solid solution, and dispersion [8-11]. HSLA steels are classified according to their composition, properties, manufacturing method, microstructure, strength, and heat treatment. Categories include weathering steels, laminated pearlitic structural steels, acicular ferrite steels, dual-phase steels, and ferritic-pearlitic microalloyed steels used in petrochemical transport, construction, and bearings [12,13].

This kind of steels are often welded using arc welding techniques (SMAW-GMAW-FCAW). During the welding process, the supplied heat produces differentiated zones that affect the microstructure and, therefore, final mechanical properties of the welded joint [14-17]. One the most used arc-welding process is gas metal arc welding – GMAW, due to highest production rate [2]. In the GMAW process, the shielding gas not only affects the welding properties but also determines the shape and pattern of penetration [18,19]. Two main categories of gases are commonly used: active and inert [20]. The most common shielding gas used in GMAW for carbon steel applications is an Ar-CO₂ mixture, with commercial mixtures ranging from 8 to 25% CO₂ [21]. The addition of CO₂ helps to stabilize the arc, and spray transfer can be achieved when up to 20% is added [22]. The addition of CO₂ increases the deposition rate of the filler material when added between 5 and 15% to pure Ar [23,24]. Adding more than 15% CO₂ to the gas mixture with Ar can result in arc instability and the production

Evaluation of the Effect of Heat Input on Welded Joint Properties of ASTM A572
Grade 50 Steel Using the GMAW Process with 90Ar-10CO2 Shielding Gas and
Spray Metal Transfer

Díaz Ávila et al.

of fumes and spatter. On the other hand, a mixture with more than 10% CO_2 increases the current density and reduces the anodic contact on the drop surface, causing repulsive forces [21].

The phase transformation of HSLA steel welding metal is complex, and its final microstructure depends on the chemical composition and cooling rate of the welding metal [15,25]. Ullah Khan et al. [26] studied the GMAW welding of HSLA steel and found that the average hardness oscillated (increased and decreased) from the weld bead to the base material. This is due to recrystallization, tempered, and the formation of martensite, retained austenite, and acicular ferrite during cooling after the joining process. The strength of the base material was higher than welded regions due to the heterogeneity in their microstructures. Ragu et al. [27] studied the effect of process parameters of welding on the tensile properties of naval grade HSLA steel welded by SMAW, GMAW, and FSW. The strength of the FSW welded joint was higher than that of the other two process, due to no fusion problems, low peak temperatures, and deformations generated during the joining process. Zhou et al. [18] correlated the heat input, microstructure, and properties in the HAZ of welded joints of ASTM A572 grade 65 steel for two different heat inputs. The width of the HAZ was proportional to the input. For both cases, the HAZ microstructure consisted of martensite and ferrite that was located at the grain boundary of the previous austenite. The joint hardness decreased continuously from the HAZ to the base material. Ebrahimnia et al. [19] studied how the composition of the shielding gas affects the welding properties of ST 37-2 steel. They evaluated four gas mixtures (97.5% Ar + 2.5% CO_2, 90% Ar + 10% CO_2, 82% Ar + 18% CO_2, and 75% Ar + 25% CO_2) influences on the microstructure of the weld metal, joint toughness, and welding pool shape. They found that the energy absorbed measured with Charpy impact test increases and then remains constant with the increase of CO_2 in the shielding gas composition. The amount of inclusions decreases and the volume fraction of Widmanstatten ferrite increases with increasing CO_2. The depth of the fusion zone in GMAW also increases with the increase of CO_2 in the shielding gas. In HSLA welded joints using GMAW increased their toughness when Ar-CO_2 mixtures were used, due to the minimization of inclusions and equilibrium of metastable tempered phases and acicular ferrite [28]. Likewise, the use of an Ar-10%CO_2 mixture during GMAW allowed an increase in droplet diameter without affecting thermal efficiency and heat distribution [29]. The mixture of Ar-10%CO_2 reduced the oxidizing and increased the melting efficiency of the consumable electrode and the base metal [22].

This investigation presents an analysis of the GMAW effects on the mechanical properties of welded joints of ASTM A572 grade 50 steel, a highly demanded steel in civil applications [30-32]. A 90% Ar + 10% CO_2 shielding gas was used to deposit filler metal using the spray transfer mode. Spray is preferred in industries because it offers uniform transfer, low spatter, high weld penetration, and lower smoke production than other modes during steel welding [33,34]. There were established relationships among microstructure evolution, microhardness, and tensile properties of the welded joints. This investigation aims to obtain results that can be applied to industries that require rapid production of welded structures and serve as a basis for future investigations addressing topics such as corrosion and fracture toughness in welded joints of this type of steel.

2. Materials and Methods

2.1. Experimental setup and materials

The experimental setup shown in Figure 1a was implemented to carry out the automatic GMAW welding process. A device was adapted to hold the torch on a Víctor® electromechanical cart to control its displacement speed during the process. Welding coupons with dimensions of 200×150×6.35 mm were extracted from commercial rolled plates, as shown in Figure 1b. The chemical composition of the base material was experimentally determined using optical emission spectroscopy, and the mechanical properties of the base material were determined through tensile tests. The results are shown in Table 1. The plates were prepared with a "V" type bevel, 60º angle, 2mm root face, and 2mm root opening according to the AWS D1.1 2020 code [35] (Figure 1c) and welded in the 1G position. A glass fiber backing and run-off plates were used.

A 256 Power MIG welding machine was used. SuperArc® LA-90 wire was used as the filler metal, whose chemical composition and mechanical properties were taken from AWS A5.28/A5.28M:2022 standard [36] and are shown in Table 2. The certified shielding gas composition for the GMAW process was 90% argon and 10% CO_2.

Table 1. Chemical composition weight (%) and mechanical properties of experimental ASTM A572 Grade 50 steel.

Chemical composition						
C	Si	Mn	P	S	Nb	Fe
0.184	0.261	1.501	0.015	0.0085	0.011	Balance
Mechanical properties						
Yield strength [MPa]		Ultimate strength [MPa]			%Elongation	
410		579.66			21.63	

Evaluation of the Effect of Heat Input on Welded Joint Properties of ASTM A572
Grade 50 Steel Using the GMAW Process with 90Ar-10CO2 Shielding Gas and
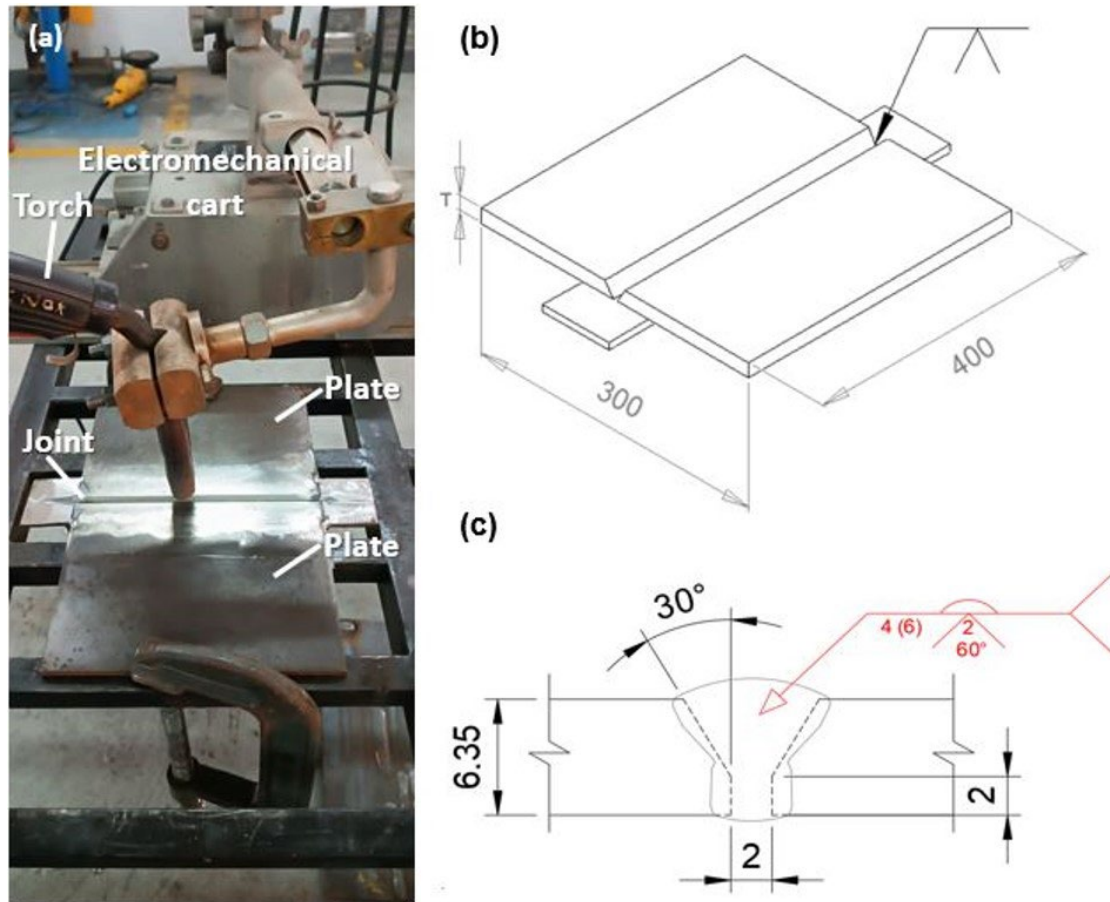Spray Metal Transfer

Díaz Ávila et al.

Figure 1. (a) Setup for semi-automated GMAW welding, (b) Welding coupon assembly, (c) Cross-sectional view of the welding coupons.

Table 2. Chemical composition weight (%) and mechanical properties of ER90S filler wire.

Chemical composition								
C	Mn	Si	Ni	Mo	S	P	Cu	Fe
0.07-0.12	1.6-2.1	0.5-0.8	0.15*	0.4-0.6	0.025*	0.025*	0.5*	Balance
Mechanical properties								
Yield strength [MPa]			Ultimate strength [MPa]			%Elongation		
620-650			705-730			25-26		

* Maximum percentage allowed per element in the filler wire.

2.2. Welding parameters

The current and voltage were adjusted according to Table 3 for the gas mixture and filler wire, in order to achieve spray transfer of the filler metal [18,21]. Two heat inputs were used, referred to as Low (L-HI) and High (H-HI), with numerical differences between them greater than 10%. Prior parameterization was performed by varying conditions. For the L-HI heat input, a stick-out of 22 mm, a welding speed of 4.4 mm/s, a wire feed speed of 122.77 mm/s, and a shielding gas flow of 22 L/min were used. In the case of H-HI, a stick-out of 19 mm, a welding speed of 3.5 mm/s, a wire feed speed of 105.83 mm/s, and a shielding gas flow of 25 L/min were used. The current and voltage intensity data in the welding process were measured in real-time using a data acquisition software called WELDVIMONOTORING® developed by Universidad Autónoma del Caribe. The setup is shown in Figure 2.

Table 3. Parameters for welding operation to obtain spray transfer.

Voltage [V]	Current [A]	Wire diameter [mm]
23 – 32	195 – 430	0.9 – 1.6

Evaluation of the Effect of Heat Input on Welded Joint Properties of ASTM A572
Grade 50 Steel Using the GMAW Process with 90Ar-10CO2 Shielding Gas and
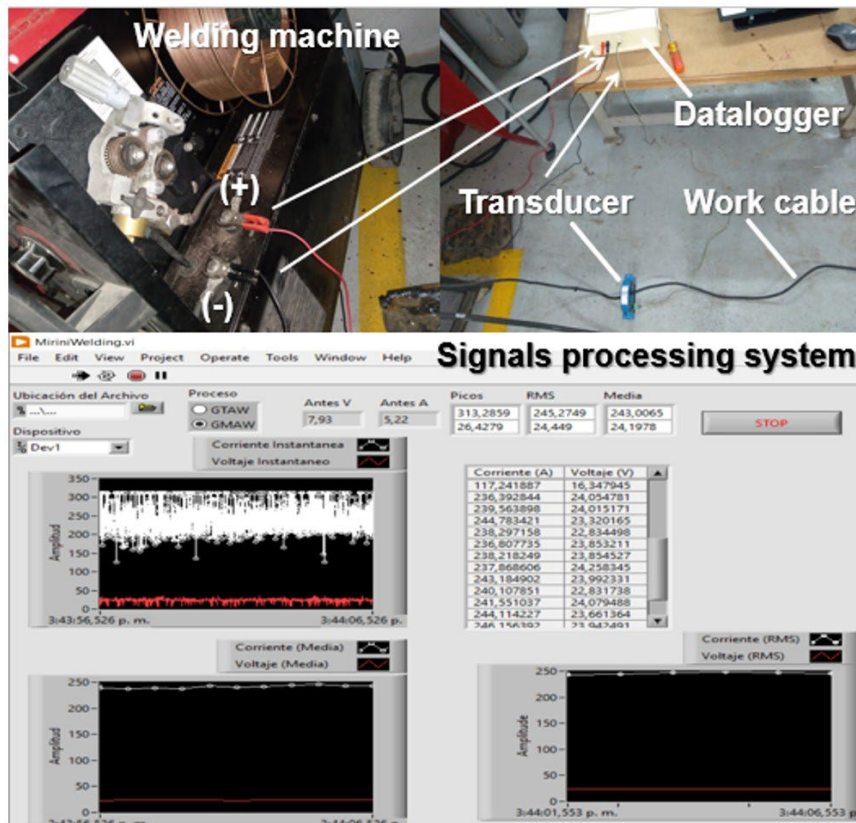Spray Metal Transfer

Díaz Ávila et al.

Figure 2. Assembly of WELDVIMONOTORING data acquisition system.

2.3. Metallographic examination of weld regions

In Figure 3 are shown the location of the metallographic, microhardness, and tensile specimens. Water jet cutting was used to extract samples from the welded joints to avoid altering their properties. Typical metallographic preparation was carried out according to ASTM E3-11 [37] standard, using 1μm alumina in polishing. The phases were revealed using 5% Nital. To obtain macrographs of the welded joints, a Motic® SMZ 171 stereoscope was used at magnifications between 2.5x and 7x, and the OMAX® ToupView software for dimensional analysis of macrographs. Microstructure was explored using an Olympus® PM3B optical microscope. X-ray diffraction patterns of different zones of the welded joints were obtained using a XPERT PRO diffractometer with a Cu-Kα wavelength of λ = 1.5406 Å, 40 kV and 30 mA, and scanning 2Θ from 20° to 134° with a step of 0.1180°, aiming to identify phases on Fusion zone (FZ).

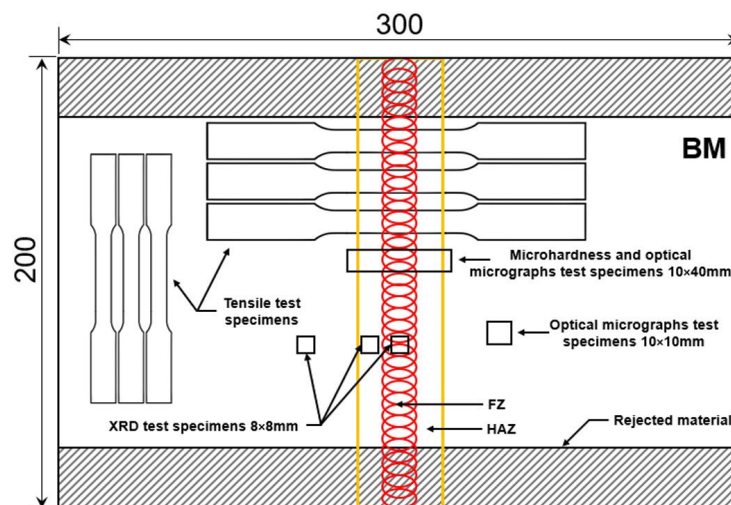**Figure 3.** Extraction of specimens for the different tests.

Evaluation of the Effect of Heat Input on Welded Joint Properties of ASTM A572
Grade 50 Steel Using the GMAW Process with 90Ar-10CO2 Shielding Gas and
Spray Metal Transfer

Díaz Ávila et al.

2.4. Measurement of mechanical properties

Tension tests were carried out using a MTS® Criterion Model 45 universal testing machine. Three samples (for repeatability) were extracted using water jet cutting from the base metal and perpendicular to welded joint regions for both heat input configurations, as is shown in Figure 3. During the tensile test was used a stroke speed of 0.06 mm/s and an extensometer MTS 634.12f-24 of 25 mm (1in). Tensile tests were conducted on the welded joints and base metal by the ASTM E8/E8M-21 standard [38]. Microhardness tests were performed using an HSV-1000A Microhardness Tester. A load of 500 g was used with a dwell time of 10 seconds. Microhardness samples were prepared according to the ASTM E92-17 standard [39]. Figure 4 shows the arrangement of the microhardness scan profiles.
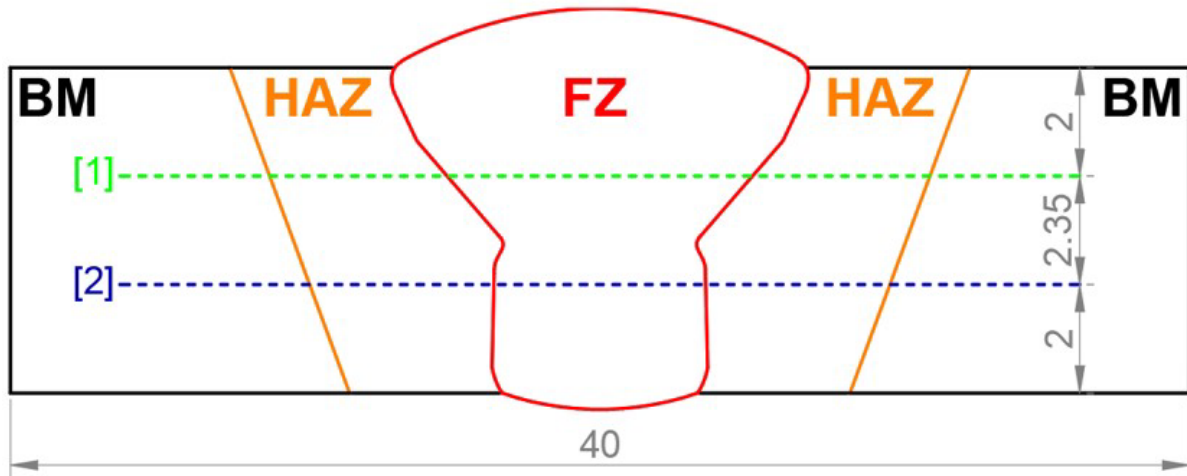

Figure 4. Microhardness scans for the welded joints.

2.5. Computational simulation of thermal history and phase transformations

Computational simulations were conducted using experimental parameters to determine the different thermal cycles and phase transformations associated with the heat-affected zone (HAZ) under welding conditions. To calculate the projected thermal cycles based on the physical parameters of the material to be welded and welding parameter information shown in Table 4, a non-commercial software called HISTOSOLD® was utilized [40]. In addition, for the phase transformations, the computational thermodynamics software JMat-Pro® was employed, which utilized the chemical composition of the base material and the estimated CCT curve using the Fe-data database. The obtained information from calculations was then compared with the experimental measurements, such as hardness, microscopic observation, and phases present in the HAZ for each welding condition.

Table 4. Physical parameters of ASTM A572 Grade 50 steel and welding parameters.

Parameters	H-HI	L-HI
Melting Temperature (°C)	1504	1504
Plate temperature (°C)	30	30
Thermal diffusivity (m^2/s)	1.58×10^{-5}	1.58×10^{-5}
Plate thickness (m)	0,00635	0,00635
Plate density (kg/m^3)	7900	7900
Specific heat capacity (J/kg°C)	424	424
Travel speed (m/s)	0.0035	0.00443
Heat input (J/m)	124300	104000

3. Results and Discussion

3.1. Determination of welding parameters and heat input

To determine the heat input in the welding process, the experimentally determined values of voltage, current intensity, welding speed, and GMAW process efficiency shown in Table 4 were taken into account. The following Equation 1 was used for the calculation:

Evaluation of the Effect of Heat Input on Welded Joint Properties of ASTM A572
Grade 50 Steel Using the GMAW Process with 90Ar-10CO2 Shielding Gas and
Spray Metal Transfer

Díaz Ávila et al.

$$Heat\ input = \left(\frac{V*I}{S*1000}\right)*\eta \text{ in kJ/mm} \tag{1}$$

Where: V = Voltage (V), I = Welding current (A), S = travel speed (mm/s), η = thermal efficiency for the welding process.

Two heat inputs were obtained, identified as high heat input (H-HI) and low heat input (L-HI). The numerical value of heat input was obtained considering an 80% efficiency in the welding process, which corresponds to the average value reported by several authors, who refer to a thermal efficiency of the GMAW process between 0.70 and 0.90 [41,42]. Table 5 shows the values of the heat inputs for the two joint configurations, H-HI and L-HI, being 1.24 kJ/mm and 1.04 kJ/mm, respectively. A numerical difference of approximately 16% is evident between them.

Table 5. Heat inputs for the two joint configurations.

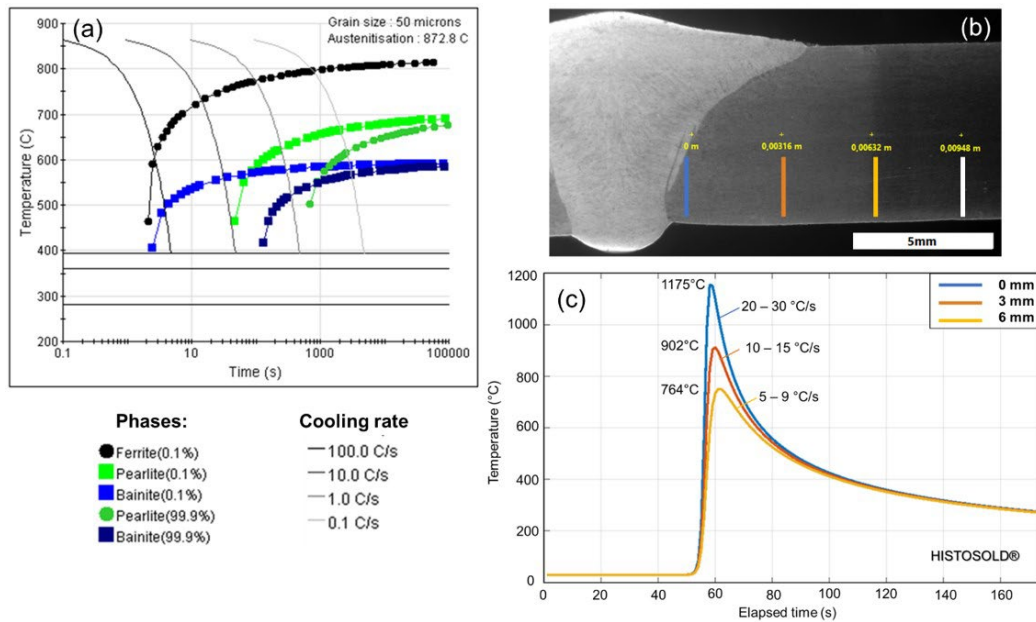| Sample		Current [A]	Voltage [V]	Travel speed [mm/s]	Wire speed [mm/s]	Heat input [kJ/mm]	Average HI (kJ/mm)
H-HI	1	223.1	24.11	3.5	105.83	1.23	1.24
	2	221.5	24.29	3.5	105.83	1.23	
	3	228.3	24.3	3.5	105.83	1.27	
L-HI	1	228.7	24.15	4.43	122,77	1.00	1.04
	2	247.8	24.24	4.43	122.77	1.08	
	3	239.8	23.99	4.43	122.77	1.04	

Each coupon was visually inspected and no presence of pores was found, and complete penetration was achieved. Additionally, there was no excessive undercut, spatter, and no superficial cracks were observed, as shown in Figure 5. The obtained welded joints were of good quality with continuous beads since no interruption in the arc occurred and all established parameters were kept constant.
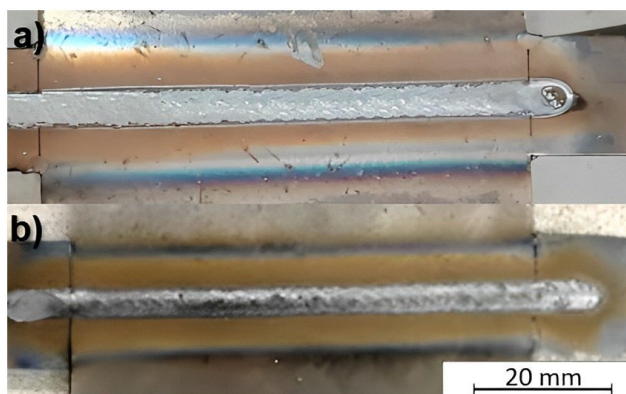
Figure 5. Welded joints (a) H-HI and (b) L-HI.

3.2. Thermal history and phase transformations analysis

Figure 6 are summarized the graphical results of the simulation thermal history and phase transformations analysis obtained using the parameters and welding conditions of this work. This first approach was developed using a CCT diagram of base metal (BM), which was calculated using commercial software based on thermodynamics phase transformation and from chemical composition shown in Table 1. Therefore, results are restricted to the HAZ region. It can be noticed that the critical cooling rate of the CCT diagram is higher than 150°C/s, which is an atypical value for HSLA steel welding. In a wide range between 0.1 to 100 °C/s is expected formation of Ferrite, Bainite, and Perlite, as is shown in Figure 6a. Attempting to establish relationships between real HAZ location and thermal cycles predicted obtained by non-commercial software based on heat distribution, there were located points in the HAZ of the cross-section of the welded joint, as shown in Figure 6b. Thermal cycles and peak temperatures obtained for these locations are displayed in Figure 6c. It can be noticed that the cooling rate of HAZ was calculated between 5 to 30 °C/s, which are reasonable values for steel welding [43,44]. When the information between the CCT diagram and welding cooling rates are crossed (i.e. Figures 6a and 6b), it is predicted that in the HAZ near close to the fusion line is predominated a microstructure formed by a combination of ferrite and bainite with a range hardness between 220 to 250 HV after cooling. At the middle of the HAZ is obtained Ferrite + Bainite + Perlite with a range hardness between 200 to 220 HV. Finally, at the HAZ near close to base metal is probably obtained Ferrite + Bainite + Perlite with range hardness between 180 to 200 HV, which are coherent with similar results obtained in the other works [45].

Evaluation of the Effect of Heat Input on Welded Joint Properties of ASTM A572
Grade 50 Steel Using the GMAW Process with 90Ar-10CO2 Shielding Gas and
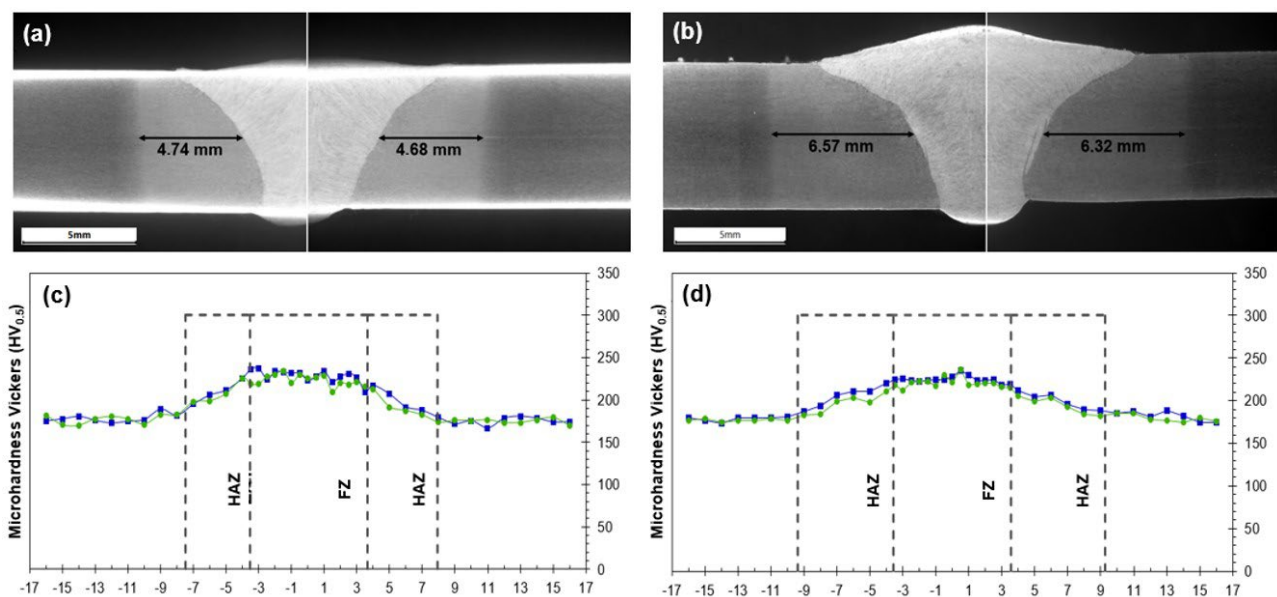Spray Metal Transfer

Díaz Ávila et al.

Figure 6. Simulation results of phase transformation in the HAZ region. (a) CCT diagram of ASTM A572-Gr50. (b) Welded joint showing location analyzed in the HAZ region. (c) Thermal cycles in HAZ locations
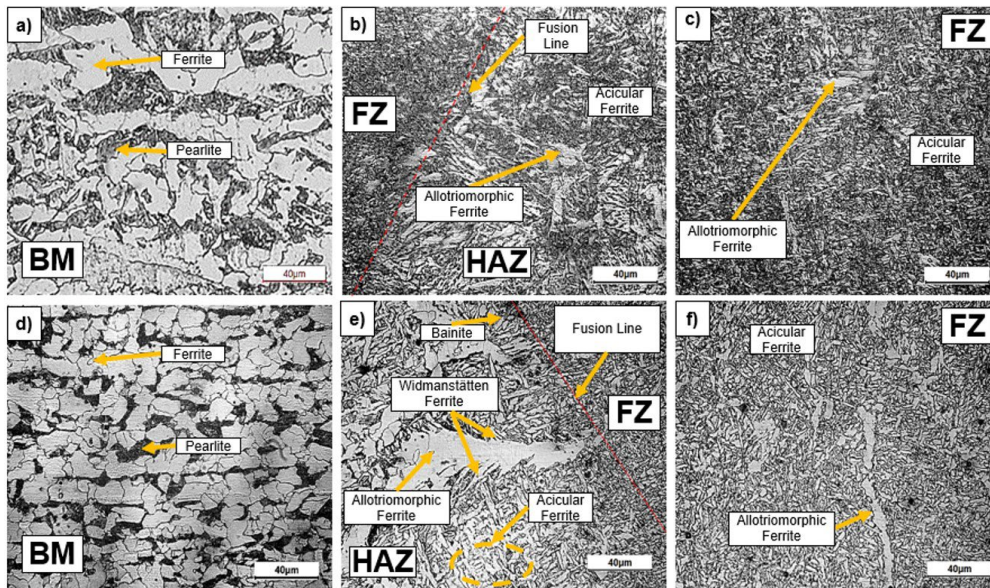
3.3. Microstructure and microhardness analysis

In Figure 7, macrographs of the welded joints for the two heat inputs are shown. the average width of the HAZ was determined, obtaining 4.72 mm for L-HI and 6.45 mm for H-HI as shown in Figures 7a and 7b, respectively. There is an approximate 26.82% difference in the HAZ width, which can be explained by the increasing base metal affectation as the heat input in the process increases [19,22].

Regarding the micrographs, phase transformations along the weld bead are evident for both heat inputs. Similar micrographs are observed for both heat inputs, where in the base material, elongated ferrite grains and pearlite colonies are observed due to the rolling process that the material undergoes for its delivery state, as shown in Figures 8a and d. In the HAZ, there was evidenced the presence of acicular ferrite, allotriomorphic ferrite, Widmanstatten ferrite, and bainite, as shown in Figures 7b and e. In Figures 8c and f are evidenced that in the fusion zone (FZ), there is a large amount acicular ferrite and allotriomorphic ferrite, which are more refined than observed in the HAZ. Similar results were found in the literature. Arista et al. [46] performed GMAW welding on a similar HSLA steel and they found the presence of Widmanstatten ferrite in the HAZ, while Da Silva et al. [47] who also performed GMAW welding on this steel, found that in the fusion zone, the predominant microstructures were acicular ferrite and allotriomorphic ferrite.

Figure 7. Macrographs at 0.75X: a) L-HI, b) H-HI; Microhardness traverse: c) L-HI, d) H-HI.

Evaluation of the Effect of Heat Input on Welded Joint Properties of ASTM A572
Grade 50 Steel Using the GMAW Process with 90Ar-10CO2 Shielding Gas and
Spray Metal Transfer

Díaz Ávila et al.

Figure 8. Micrographs at 500X of the joint L-HI: a) BM, b) HAZ, c) FZ; Micrographs at 500X of the joint H-HI: d) BM, e) HAZ, f) FZ. BM: base metal, HAZ: heat affected zone. FZ: fusion zone.

Microhardness profiles results (Figures 7c and 7d) showed a constantly increasing trend from base metal to fusion zone for both applied heat input. Maximum values for each welding region did not show significant differences in each case. In the HAZ for both H-HI and L-HI configurations, microhardness values of 206.08 ± 14.7 HV, and 201.83 ± 12.3 HV were obtained, respectively, while in the FZ, values of 220.29 ± 12.5 HV, and 214.31 ± 12.7 HV were obtained, respectively. The Base metal showed an average hardness of 177.5 ± 4.5 HV, which is a similar value reported in the literature [48,49]. Compared to the base metal, the hardness of HAZ and FZ regions increased between 15 to 25%, respectively. Microstructure observations evidenced a predominance of acicular structures in the FZ region, while a combination of ferrite, bainite, perlite, and little bits of acicular structures are displayed in the HAZ region from fusion line to non-heat affected base metal, such as is shown in the Figures 8a to 8f. These aforementioned results are consistent with simulation results for the HAZ microstructure evolution in accordance cooling rate undergone in the function of distance to the fusion line (See Figure 5).

The presence of bainite and acicular microstructures in the HAZ region are responsible for the hardness increase, while the chemical composition of filler metal, dilution, and acicular ferrite presence can explain the obtained maximum value of hardness in the fusion zone. Bainite has a finer structure and therefore exhibits greater strength and hardness than the base material, while the presence of acicular ferrite favors increasing of the strength of the welded joint. Acicular ferrite is a highly substructured non-equiaxed phase with highly dense cross-linked dislocations anchored by fine carbonitride particles [50]. Additionally, fine carbonitride particles within the acicular ferrite provide a significant reinforcement effect for HSLA steels [50,51].

3.4. X-Ray Diffraction analysis

The x-ray diffraction (XRD) spectral were obtained for non-welded base metal (BM) and the fusion zone (FZ) of the welded joints with both heat inputs H-HI and L-HI (see Figure 9).
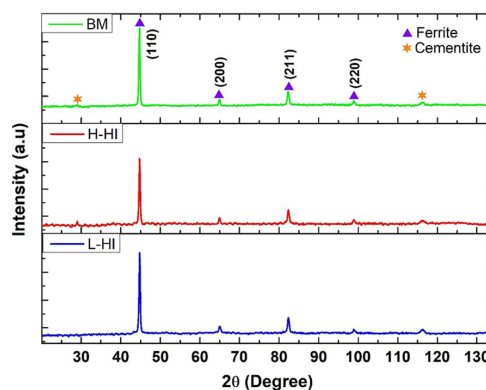
Figure 9. Diffraction patterns: base metal (BM), high heat input weld metal (H-HI) and low heat input weld metal (L-HI).

Evaluation of the Effect of Heat Input on Welded Joint Properties of ASTM A572
Grade 50 Steel Using the GMAW Process with 90Ar-10CO2 Shielding Gas and
Spray Metal Transfer

Díaz Ávila et al.

XRD analysis obtained for ASTM A572 Gr 50 steel show detected peaks corresponding to ferrite and Cementite (Fe_3C), the latter being present in the pearlitic microconstituent. On the other hand, XRD analysis of FZ of the welded joints show the predominance of ferrite, which is coherent with microstructure analysis. Peaks corresponding to Cementite (Fe_3C) are also evident, which are attributed to the presence of the bainitic phase in the fusion zone. According to the diffraction patterns in the HAZ of the welded joints with low heat input, there is a lower volumetric fraction of Fe_3C, as the peaks of this phase have a lower intensity compared to those present in the diffraction pattern of the welded joints with high heat input [52,53].

3.5. Tensile tests result analysis

Figure 10 shows the comparison among tensile test results for non-welded base metal and welded joints. It is noticed that curves show similar trends with a ductile predominant behavior. L-HI and BM curves show a soft transition from elastic to plastic portion, while the H-HI curve shows a stress plateau (flow configuration) in the yield strength region. This aforementioned behavior can be related to typical C-Mn steels response to high dislocations concentration during uniaxial deformation [54,55].
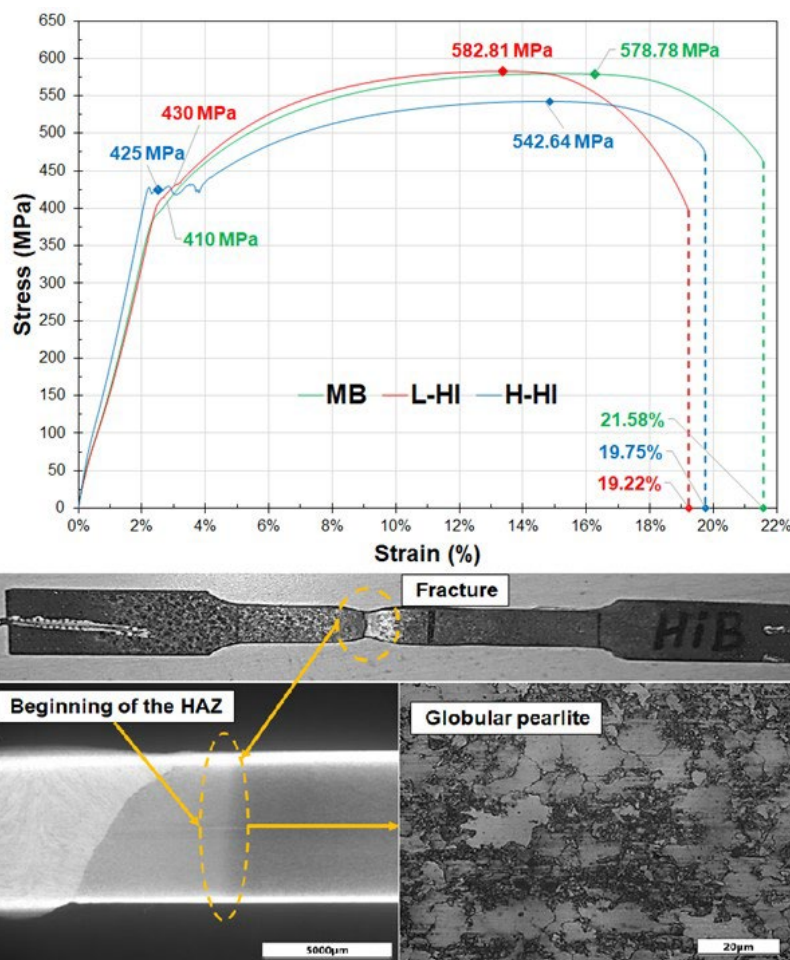

Figure 10. Stress vs. strain diagram and tensile test specimen fractured at the beginning of the HAZ.

For welded tensile specimens have been determined that the fracture occurred at the beginning of the HAZ where globular pearlite predominates, as is shown in Figure 10. Globular pearlite is formed during a short time of annealing of Low alloy steel [56], which was possible to obtain in the boundary between HAZ and BM region by thermal conditions there experienced. According to [57], the globular pearlite phase in steels shows much lower strength than laminar pearlite steels despite having the same fraction of cementite. The yield strength values of the base metal, L-HI, and H-HI were 410 MPa, 430 MPa, and 425 MPa respectively. Besides, the ultimate tensile strength values were 578.78 MPa, 582.81 MPa, and 542.64 MPa respectively. Finally, percentage elongation of 19.75% and 19.22% were obtained for L-HI, and H-HI, respectively, which were not significantly different to 21.58% showed by base metal. Figure 8 shows that the base material has a higher percentage of elongation due to its homogeneous microstructure, unlike the welded samples which have a variable microstructure along the HAZ regions. In other work [58], it was obtained lower ultimate strength ($S_u \sim$ 390 MPa) in welded joints developed on the same kind of steel (ASTM A572) using the GMAW process and ER70S-6 filler metal.

Evaluation of the Effect of Heat Input on Welded Joint Properties of ASTM A572
Grade 50 Steel Using the GMAW Process with 90Ar-10CO2 Shielding Gas and
Spray Metal Transfer

Díaz Ávila et al.

4. Conclusions

From the obtained results of the evaluation of welded joints of ASTM A572-Gr50 HSLA steel GMAW using 90Ar-10CO2 shielding gas and ER90S6 wire rode electrode in spray transfer mode with two heat inputs, it can be possible to deduce the following remark conclusions:

- It was enabled to develop welded joints discontinuities-free, with full penetration using a one-pass welding bead, without excessive undercut, spatter, and no superficial cracks;

- Mechanical properties of welded joints exhibited maximum tensile strength and hardness value higher than base metal mainly due to acicular structures observed in the fusion zone;

- Regarding base metal, a slight decrease of ductility was observed in the welded joints due to the heterogeneity of phases and their contribution during deformation in the HAZ region;

- The observed microstructures at the different welded regions were coherent with the results of the thermal simulation. The CCT diagram of ASTM A572 steel was useful to estimate the phases present in the HAZ.

Authors' contributions

JUS: Project administration, resources, supervision, funding acquisition, investigation, visualization, writing – review & editing, and formal analysis. EENN: resources, funding acquisition, investigation, visualization, writing – review & editing, and formal analysis. ÁMDÁ: investigation, visualization, writing – original draft, validation, data curation, and formal analysis. EJHO: investigation, visualization, writing – original draft, validation, data curation, and formal analysis. ECMP: investigation, visualization, writing – original draft, validation, data curation, and formal analysis.

Acknowledgements

References

[1] Pradeep Kumar P, Santos DA, Braham EJ, Sellers DG, Banerjee S, Dixit MK. Punching above its weight: life cycle energy accounting and environmental assessment of vanadium microalloying in reinforcement bar steel. Environmental Science. Processes & Impacts. 2021;23(2):275-290. http://dx.doi.org/10.1039/D0EM00424C. PMid:33355560.

[2] Jindal S, Chhibber R, Mehta NP. Issues in Welding of HSLA steels. Advanced Materials Research. 2011;365:44-49. http://dx.doi.org/10.4028/www.scientific.net/AMR.365.44.

[3] Vervynckt S, Verbeken K, Lopez B, Jonas JJ. Modern HSLA steels and role of non-recrystallisation temperature. International Materials Reviews. 2012;57(4):187-207. http://dx.doi.org/10.1179/1743280411Y.0000000013.

[4] Li X, Shi L, Liu Y, Gan K, Liu C. Achieving a desirable combination of mechanical properties in HSLA steel through step quenching. Materials Science and Engineering A. 2019;138683. http://dx.doi.org/10.1016/j.msea.2019.138683.

[5] Costa e Silva A. Challenges and opportunities in thermodynamic and kinetic modeling microalloyed HSLA steels using computational thermodynamics. Calphad. 2020;68:101720. http://dx.doi.org/10.1016/j.calphad.2019.101720.

[6] Almatani RA, DeArdo AJ. Rational alloy design of niobium-bearing HSLA steels. Metals. 2020;10(3):413. http://dx.doi.org/10.3390/met10030413.

[7] Silveira JW, Resende M. Competition in the international niobium market: a residual demand approach. Resources Policy. 2020;65:101564. http://dx.doi.org/10.1016/j.resourpol.2019.101564.

[8] Park D-B, Huh M-Y, Shim J-H, Suh J-Y, Lee K-H, Jung W-S. Strengthening mechanism of hot rolled Ti and Nb microalloyed HSLA steels containing Mo and W with various coiling temperature. Materials Science and Engineering A. 2013;560:528-534. http://dx.doi.org/10.1016/j.msea.2012.09.098.

[9] Frátrik M, Mičian M, Winczek J. An analysis of strengthening mechanisms of TMCP HSLA steels. Proceedings of the 27/28 International Conference Engineering Mechanics 2022; 2022 May 9-12; Milovy, Czech Republic. Prague: IMCE. p. 113-116. Paper 97. http://dx.doi.org/10.21495/51-2-113.

[10] Tomków J. Weldability of Underwater Wet-Welded HSLA Steel: Effects of Electrode Hydrophobic Coatings. Materials (Basel). 2021;14(6):1364. http://dx.doi.org/10.3390/ma14061364. PMid:33799785.

Evaluation of the Effect of Heat Input on Welded Joint Properties of ASTM A572
Grade 50 Steel Using the GMAW Process with 90Ar-10CO2 Shielding Gas and
Spray Metal Transfer

Díaz Ávila et al.

[11] Sun L-Y, Liu X, Xu X, Lei S-W, Li H-G, Zhai Q-J. Review on niobium application in microalloyed steel. Journal of Iron and Steel Research International. 2022;29:1513-1525. http://dx.doi.org/10.1007/s42243-022-00789-1.

[12] Olorundaisi E, Jamiru T, Adegbola AT. Mitigating the effect of corrosion and wear in the application of High Strength low Alloy Steels (HSLA) in the petrochemical transportation industry - a review. Materials Research Express. 2019. http://dx.doi.org/10.1088/2053-1591/ab65e7.

[13] Morales EV. Alloy steel – properties and use. London: Intechopen; 2011.

[14] Bose-Filho WW, Carvalho ALM, Strangwood M. Effects of alloying elements on the microstructure and inclusion formation in HSLA multipass welds. Materials Characterization. 2007;58(1):29-39. http://dx.doi.org/10.1016/j.matchar.2006.03.004.

[15] Alipooramirabad H, Paradowska A, Ghomashchi R, Reid M. Investigating the effects of welding process on residual stresses, microstructure and mechanical properties in HSLA steel welds. Journal of Manufacturing Processes. 2017;28:70-81. http://dx.doi.org/10.1016/j.jmapro.2017.04.030.

[16] Hariprasath P, Sivaraj P, Balasubramanian V, Srinivas Pilli K. Effect of welding processes on high cycle fatigue behavior for naval grade HSLA joints: a fatigue strength prediction. Engineering Failure Analysis. 2022;142:106783. http://dx.doi.org/10.1016/j.engfailanal.2022.106783.

[17] Duprez, L., Leunis, E., Güngör, Ö. E., & Claessens, S. Hydrogen embrittlement of high strength, low alloy (HSLA) steels and their welds. In: Gangloff RP, Somerday BP, editors. Gaseous hydrogen embrittlement of materials in energy technologies. Sawston: Woodhead Publishing Limited; 2012. p. 562-591. http://dx.doi.org/10.1533/9780857093899.3.562.

[18] Zhou JL, Yang JH, Ye Y, Dai GP, Peng XY. Effect of heat input on microstructure and properties in heat affected zone of ASTM A572 GR.65 steel. Advanced Materials Research. 2010;148-149:553-557. http://dx.doi.org/10.4028/www.scientific.net/AMR.148-149.553.

[19] Ebrahimnia M, Goodarzi M, Nouri M, Sheikhi M. Study of the effect of shielding gas composition on the mechanical weld properties of steel ST 37-2 in gas metal arc welding. Materials & Design. 2009;30(9):3891-3895. http://dx.doi.org/10.1016/j.matdes.2009.03.031.

[20] Pattanayak S, Sahoo SK. Gas metal arc welding based additive manufacturing: a review. CIRP Journal of Manufacturing Science and Technology. 2021;33:398-442. http://dx.doi.org/10.1016/j.cirpj.2021.04.010.

[21] de Meneses VA, Leal VS, Scotti A. Influence of metal transfer stability and shielding gas composition on CO and CO_2 emissions during short-circuiting MIG/MAG welding. Soldagem e Inspeção. 2016;21(3):253-268. http://dx.doi.org/10.1590/0104-9224/SI2103.02.

[22] Mvola B, Kah P. Effects of shielding gas control: welded joint properties in GMAW process optimization. International Journal of Advanced Manufacturing Technology. 2016;88(9-12):2369-2387. http://dx.doi.org/10.1007/s00170-016-8936-2.

[23] Rhee S, Kannatey-Asibu JE. Observation of metal transfer during gas metal arc welding. Welding Journal. 1992;71:381-386.

[24] Rice VJ. Initial testing for the recommendation of improved gas metal arc welding procedures for HY-80 steel plate butt joints at norfolk naval shipyard [master's thesis]. Monterey: Naval Postgraduate School Monterey; 2015.

[25] Zhang T, Li Z, Young F, Kim HJ, Li H, Jing H, et al. Global progress on welding consumables for HSLA steel. ISIJ International. 2014;54(7):1472-1484. http://dx.doi.org/10.2355/isijinternational.54.1472.

[26] Ullah Khan N, Rajput SK, Gupta V, Verma V, Soota T. To study mechanical properties and microstructures of MIG welded high strength low alloy steel. Materials Today: Proceedings. 2019;18:2550-2555. http://dx.doi.org/10.1016/j.matpr.2019.07.112.

[27] Ragu Nathan S, Balasubramanian V, Malarvizhi S, Rao AG. Effect of welding processes on mechanical and microstructural characteristics of high strength low alloy naval grade steel joints. Defence Technology. 2015;11(3):308-317. http://dx.doi.org/10.1016/j.dt.2015.06.001.

[28] Bird J. Improving the toughness of high strength GMA welds. Marine Structures. 1993;6(5-6):461-474. http://dx.doi.org/10.1016/0951-8339(93)90032-X.

[29] McIntosh C, Chapuis J, Mendez PF. Effect of Ar-CO2 gas blends on droplet temperature in GMAW. Welding Journal. 2016;95(8):273s.

[30] Aziz EM, Kodur VK. Effect of temperature and cooling regime on mechanical properties of high-strength low-alloy steel. Fire and Materials. 2016;40(7):926-939. http://dx.doi.org/10.1002/fam.2352.

[31] Sajid HU, Kiran R. Influence of high stress triaxiality on mechanical strength of ASTM A36, ASTM A572 and ASTM A992 steels. Construction & Building Materials. 2018;176:129-134. http://dx.doi.org/10.1016/j.conbuildmat.2018.05.018.

[32] Chi J-H, Peng P-C. Study of the structural safety assessment of steel bridge subjected in post-fire. Construction & Building Materials. 2020;247:118587. http://dx.doi.org/10.1016/j.conbuildmat.2020.118587.

[33] Dos Santos EBF, Pistor R, Gerlich AP. High frequency pulsed gas metal arc welding (GMAW-P): the metal beam process. Manufacturing Letters. 2017;11:1-4. http://dx.doi.org/10.1016/j.mfglet.2017.01.001.

[34] Vairamani V, Mohan N, Venkatesh, Karthikeyan SK, Sakthivel M. Optimization and microstructure analysis of Corten steel joint in mag welding by post heat treatment. Materials Today: Proceedings. 2020;21:673-680. http://dx.doi.org/10.1016/j.matpr.2019.06.737.

Evaluation of the Effect of Heat Input on Welded Joint Properties of ASTM A572
Grade 50 Steel Using the GMAW Process with 90Ar-10CO2 Shielding Gas and
Spray Metal Transfer

Díaz Ávila et al.

[35] American Welding Society. AWS D1.1/D1.1M:2020: structural welding code - steel. Miami: American Welding Society; 2020.

[36] American Welding Society. AWS A5.28/A5.28M:2022: specification for low-alloy steel electrodes and rods for gas shielded arc welding. Miami: AWS.

[37] American Society for Testing and Materials. ASTM E3-11: standard guide for preparation of metallographic specimens. West Conshohocken: ASTM International; 2017.

[38] American Society for Testing and Materials. ASTM E/E8M: standard test methods for tension testing of metallic materials. West Conshohocken: ASTM International; 2021.

[39] American Society for Testing and Materials. ASTM E92-17: standard test methods for Vickers hardness and Knoop hardness of metallic materials. West Conshohocken: ASTM International; 2017.

[40] Pacheco Y, Jorge L, Olmos MM, Chamorro CR, Unfried SJ. Modelado de ciclos térmicos durante la soldadura al arco eléctrico con electrodo revestido en juntas disímiles de aceros inoxidables usando una aproximación teórico-experimental. Revista de la Facultad de Ingeniería Universidad Central de Venezuela. 2015;30(3):111-118.

[41] Pépe N, Egerland S, Colegrove PA, Yapp D, Leonhartsberger A, Scotti A. Measuring the process efficiency of controlled gas metal arc welding processes. Science and Technology of Welding and Joining. 2011;16(5):412-417. http://dx.doi.org/10.1179/1362171810Y.0000000029.

[42] Pozo-Morejón JA, de Souza LFG, Guerra T, Morales EV, Bott IS, Cruz-Crespo A, et al. Ajuste de los calores de entrada que se corresponden con los tiempos de enfriamiento de la ZAT en soldadura GMAW Sobre Acero Dúplex 2205 empleando la simulación por elementos finitos. Soldagem e Inspeção. 2018;23(3):413-422. http://dx.doi.org/10.1590/0104-9224/si2303.10.

[43] Shome M, Mohanty ON. Continuous cooling transformation diagrams applicable to the heat-affected zone of HSLA-80 and HSLA-100 steels. Metallurgical and Materials Transactions. A, Physical Metallurgy and Materials Science. 2006;37(7):2159-2169. http://dx.doi.org/10.1007/BF02586136.

[44] Falkenreck T, Kromm A, Böllinghaus T. Investigation of physically simulated weld HAZ and CCT diagram of HSLA armour steel. Welding in the World. 2018;62(1):47-54. http://dx.doi.org/10.1007/s40194-017-0511-4.

[45] Geng X, Mao X, Wu HH, Wang S, Xue W, Zhang G, et al. A hybrid machine learning model for predicting continuous cooling transformation diagrams in welding heat-affected zone of low alloy steels. Journal of Materials Science and Technology. 2022;107:207-215. http://dx.doi.org/10.1016/j.jmst.2021.07.038.

[46] Arista BV, Flores IG, González CEC, Vargas LR, Villasana JP. On the effect of Qnet on compressive residual stresses and ductile toughness of dissimilar HAZ in robotic GMAW joints between A572-50 and A36 steels. International Journal of Advanced Manufacturing Technology. 2021;113(5-6):1535-1546. http://dx.doi.org/10.1007/s00170-021-06622-5.

[47] Da Silva MS, Souza D, de Lima EH, Bianchi KE, Vilarinho LO. Analysis of fatigue-related aspects of FCAW and GMAW butt-welded joints in a structural steel. Journal of the Brazilian Society of Mechanical Sciences and Engineering. 2019;42(1):67. http://dx.doi.org/10.1007/s40430-019-2142-8.

[48] Lim, Y. C., Sanderson, S., Mahoney, M., Yu, X., Qiao, D., Wang, Y., Feng, Z. (2013). Mechanical properties and microstructural characterization of a multilayered multipass friction stir weld in steel. In: Mishra R, Mahoney MW., Sato Y, Hovanski Y, Verma R, editors. Friction Stir Welding and Processing VII. Cham: Springer. p. 81-90. http://dx.doi.org/10.1007/978-3-319-48108-1_9.

[49] Vieira F, Al-Rubaie K, Preti O, Richter R, Delijaicov S. Impacto nas propriedades mecânicas e tensões residuais do material ASTM A572 grau 50 soldado por arco submerso com alívio de tensões térmico. Soldagem & Inspeção. 2019;24:e2431. https://doi.org/10.1590/0104-9224/SI24.31.

[50] Shao Y, Liu C, Yan Z, Li H, Liu Y. Formation mechanism and control methods of acicular ferrite in HSLA steels: A review. Journal of Materials Science and Technology. 2018;34(5):737-744. http://dx.doi.org/10.1016/j.jmst.2017.11.020.

[51] Shi L, Yan Z, Liu Y, Zhang C, Qiao Z, Ning B, et al. Improved toughness and ductility in ferrite/acicular ferrite dual-phase steel through intercritical heat treatment. Materials Science and Engineering A. 2014;590:7-15. http://dx.doi.org/10.1016/j.msea.2013.10.006.

[52] Bansal GK, Tripathy S, Chandan AK, Rajinikanth V, Ghosh C, Srivastava VC, et al. Influence of quenching strategy on phase transformation and mechanical properties of low alloy steel. Materials Science and Engineering A. 2021;826:141937. http://dx.doi.org/10.1016/j.msea.2021.141937.

[53] Hasan SM, Kumar S, Chakrabarti D, Singh SB. Effect of prior austenite grain size on the formation of carbide-free bainite in low-alloy steel. Philosophical Magazine. 2020;100(18):2320-2334. http://dx.doi.org/10.1080/14786435.2020.1764653.

[54] Liang ZY, Cao ZH, Lu J, Huang MX, Tasan CC. Influence of co-existing medium Mn and dual phase steel microstructures on ductility and Lüders band formation. Acta Materialia. 2021;221:117418. http://dx.doi.org/10.1016/j.actamat.2021.117418.

[55] Wang XG, Liu CH, He BB, Jiang C, Huang MX. Microscopic strain partitioning in Lüders band of an ultrafine-grained medium Mn steel. Materials Science and Engineering A. 2019;761:138050. http://dx.doi.org/10.1016/j.msea.2019.138050.

Evaluation of the Effect of Heat Input on Welded Joint Properties of ASTM A572
Grade 50 Steel Using the GMAW Process with 90Ar-10CO2 Shielding Gas and
Spray Metal Transfer

Díaz Ávila et al.

[56] Kaspar R, Kapellner W, Lang C. Hot deformation-enhanced globularization of pearlite. Steel Research. 1988;59(11):492-498. http://dx.doi.org/10.1002/srin.198801546.

[57] Allain SYP, Roth A, Bouaziz O, D'Eramo E. Microstructure-based behavior law for globular pearlitic steels. Journal of Materials Research and Technology. 2019;8(3):3373-3376. http://dx.doi.org/10.1016/j.jmrt.2019.03.014.

[58] Deo M, Tewari SP, Mahobia GS. Behaviour of HAZ and weld bead under different welding condition for A572 GR 50 steel. International Journal of Advanced Research in Engineering and Technology. 2020;11(6):646-655. http://dx.doi.org/10.34218/IJARET.11.6.2020.05.